Simulated observation of tropospheric ozone and CO with the Tropospheric Emission Spectrometer (TES) satellite instrument

M. Luo and R. Beer
Jet Propulsion Laboratory, California Institute of Technology, Pasadena, California, USA

D. J. Jacob and J. A. Logan
Department of Earth and Planetary Sciences, Harvard University, Cambridge, Massachusetts, USA

C. D. Rodgers
Atmospheric, Oceanic and Planetary Physics, University of Oxford, Oxford, UK

Received 30 April 2001; revised 18 September 2001; accepted 25 September 2001; published 14 August 2002.

[1] The Tropospheric Emission Spectrometer (TES) on board NASA's Aura satellite (to be launched in 2004) will provide measurements of global distributions of ozone, CO, and other key chemical species in the troposphere. In order for TES to meet a design lifetime of 5 years, it has been determined that a global survey strategy with ~50% duty cycle must be identified. In this study, simulated concentrations of ozone and CO from the GEOS-CHEM global three-dimensional (3-D) model of troposphere chemistry are used as a time-varying synthetic atmosphere for demonstrating and assessing the capabilities of TES nadir observations. Autocorrelation analyses of the model species fields for different time lags identify a significant 1-day correlation and support a 1-day-on/1-day-off observation strategy. Three major steps are then taken to demonstrate and evaluate TES products: (1) species profiles along the TES orbit track are sampled from the model 3-D time-varying fields with cloudy scenes (50-60% of total scenes) removed; (2) nadir-retrieved profiles (''level 2 products'') are obtained from these ''true'' synthetic profiles using TES retrieval characteristic functions; (3) interpolated daily global maps (''level 3 products'') are generated to compare with the original model fields. The latter comparison indicates that the error in the level 3 products relative to the true fields for ozone and CO is <10% in ~70% of cases and <20% in 80–90% of cases. The three major sources of error lie in the asynoptic orbital sampling, the retrieval, and the level 3 global mapping. *INDEX TERMS:* 0365 Atmospheric Composition and Structure: Troposphere—composition and chemistry; 0368 Atmospheric Composition and Structure: Troposphere—constituent transport and chemistry; 3360 Meteorology and Atmospheric Dynamics: Remote sensing; *KEYWORDS:* TES, tropospheric emission spectrometer, ozone, carbon monoxide, tropospheric chemistry, satellite remote sensing

1. Introduction

[2] The Tropospheric Emission Spectrometer (TES) is one of four instruments on the NASA EOS Aura satellite scheduled for launch in 2004. TES is an infrared, high spectral resolution Fourier transform spectrometer (FTS) and will operate in both nadir and limb modes to measure atmospheric profiles [*Beer et al.*, 2001]. One of the primary science objectives of TES observations is to provide concurrent measurements of vertically resolved global distributions of tropospheric ozone and some of its key precursors (CO, H_2O, NO, and HNO_3). Tropospheric ozone has been measured from space by the Global Ozone Monitoring Experiment (GOME) [*Munro et al.*, 1998]. *Fishman et al.* [1990] have reported derived tropospheric ozone columns by differencing the results from the Total Ozone Mapping Spectrometer (TOMS) and Stratospheric Aerosol and Gas Experiment (SAGE) experiments. Global CO distributions were measured four times briefly from the space shuttle by the Measurement of Air Pollution From Satellites (MAPS) experiment [*Reichle et al.*, 1999]. The Interferometric Monitor for Greenhouse Gases (IMG) instrument on board ADEOS launched in 1996 provided limited CO column measurements [*Hadji-Lazaro et al.*, 1999]. The Measurement of Pollution in the Troposphere (MOPITT) experiment on the NASA EOS Terra satellite launched in December 1999 will soon provide tropospheric CO measurements [*Drummond and Mand*, 1996].

[3] In addition to obtaining climatological data for the above-mentioned tropospheric species fields (e.g., monthly global maps) an important science goal for TES is to capture the temporal evolutions of the fields on synoptic scales, such as the export of CO from industrialized continents and the

0148-0227/02/2001JD000804$09.00

evolution of large-scale ozone episodes in the troposphere. The mechanical movement of the FTS scanning mirrors imposes a limitation on the total number of scans that TES can perform and therefore its operating lifetime. To spread the estimated total number of scans of the interferometer to its design lifetime of 5 years, the TES science team needs to develop a sampling strategy allowing the instrument to operate in roughly a 50% duty cycle. An optimal cycle frequency must be defined. *Fowler et al.* [2000] previously used the CSU GCM model to explore the sampling issues associated with remote sensing of the Earth radiation budget from multiplatform instruments. In a similar manner we use here results from the GEOS-CHEM global 3-D model of tropospheric chemistry [*Bey et al.*, 2001] to provide quantitative information about the scales of variability of the chemical fields of interest to TES and to allow us to simulate and evaluate the TES product. Our focus is on nadir observations, but the concept and the conclusions can be readily extended to the limb observations.

[4] Our approach is to use the GEOS-CHEM model to generate a synthetic "true" atmosphere and then to examine the capability of TES to retrieve this atmosphere. The advantage of using a global 3-D model to define the true atmosphere is that it provides a continuous and internally consistent global view of atmospheric composition including altitude-dependent clouds (which TES cannot see through) and variability, at least on synoptic scales. Section 2 provides an autocorrelation analysis of the GEOS-CHEM model fields, which leads to the selection of a 1-day-on/1-day-off observation pattern as the optimal way of meeting the 50% duty cycle requirement. The TES products are then simulated and evaluated in sections 3 to 5. Section 3 describes the TES-sampled profiles obtained with TES flying through the true model atmosphere. Similar to other satellite projects, TES data processing consists of levels 1, 2, and 3. Level 1 processing generates radiometric and spectrally calibrated infrared spectra from measured interferograms. Level 2 processing extracts species profiles in the atmosphere at the TES targets by fitting the spectral radiance of level 1 output with a radiative transfer model, considering the measurement errors and the reasonable physical constraints (a priori) applied in the retrievals. The level 3 processing is a step to generate global/regional images of the level 2 profiles. Section 4 describes the "fast" retrieval results (level 2 data) using TES characteristic functions with the a priori information obtained from the model yearlong data. The retrieval errors are also presented. Section 5 presents the level 3 global maps and the comparisons of these maps with the model true atmospheres. Section 6 offers a summary and some conclusions.

2. The GEOS-CHEM Model Fields

[5] The GEOS-CHEM model provides a synthetic true atmosphere for retrieval by the TES algorithm. The model is described by *Bey et al.* [2001], who also present a detailed global evaluation of model results with observations for tropospheric ozone, CO, and related species. The GEOS-CHEM model is driven by assimilated meteorological observations from the Global Earth Observing System (GEOS) of the NASA Data Assimilation Office and represents the latest generation of global 3-D models of tropospheric chemistry developed at Harvard University (earlier generations are described by *Wang et al.* [1998a, 1998b], *Horowitz and Jacob* [1999], and *Mickley et al.* [1999]). It simulates the evolution of 120 chemical species describing tropospheric ozone-NO_x-hydrocarbon chemistry. For the present application the horizontal resolution is 4° latitude × 5° longitude, with 14 vertical levels on a sigma (terrain-following) coordinate from the surface to 150 hPa. The simulation is conducted for the full year of 1994, and global fields of ozone and CO concentrations are archived every 4 hours. To facilitate the retrieval process, the model results were mapped on to 21 pressure levels between the surface and 100 hPa. As an example, Figure 1a shows a daily average ozone field from the model at 500 hPa for 15 August 1994. The simulated summertime ozone maximum in the middle troposphere over the Middle East is discussed by *Li et al.* [2001] and appears consistent with the few aircraft observations available. The ability of the TES retrieval algorithm to reproduce the concentration field in Figure 1a will be discussed in section 3.

[6] The temporal evolution of the model fields provides information toward deciding the sampling frequency needed for TES global survey observations in the context of the limitation of 50% observation duty cycle. Since TES is a polar Sun-synchronous orbit, it requires 1 day to cover the entire globe. A design requirement of TES on Aura is that it provides global survey data; therefore the limitation of 50% observation duty cycle should still allow for continuous 24-hour observation, with such observation to take place on 50% of the days. As an objective guide to design the optimal sampling strategy, we examined the autocorrelation at fixed locations of the model O_3 and CO fields for different time lags (1 day, 2 days, etc.). The autocorrelation coefficient r_k for a species at a given location for a time lag of k days is defined as

$$r_k = \sum_{t=1}^{N-k} (x_t - \bar{x})(x_{t+k} - \bar{x}) \left[\sum_{t=1}^{N} (x_t - \bar{x})^2 \right]^{-1}, \qquad (1)$$

where x_t is the model daily average O_3 or CO concentration for day t, N is the number of days considered, and $\bar{x}$ is the mean value of x_t for the N days. The relationship of 1 day's species field to that of a kth earlier day is measured by r_k.

[7] We calculated the monthly autocorrelation coefficients (N is the number of days in the month) of model ozone and CO at 800 and 500 hPa for time lags of 1, 2, and 3 days. The coefficients displayed latitudinal dependencies, compared to the global average values, ~30% higher in the tropics and 20% lower in high latitudes. At 800 hPa the global averaged monthly autocorrelation coefficients for both ozone and CO are 0.57 ± 0.04 for a 1-day time lag, 0.27 ± 0.03 for a 2-day time lag, and 0.21 ± 0.03 for a 3-day time lag. At 500 hPa the global averaged coefficients for ozone become 0.51 ± 0.04 for a 1-day time lag, 0.25 ± 0.03 for a 2-day time lag, and 0.20 ± 0.03 for a 3-day time lag, and the coefficients for CO are ~0.01 larger. These results are very close to those for afternoon ozone measurements from rural areas of the eastern United States [*Logan*, 1989].

[8] As expected, the autocorrelation coefficient for the species fields drops as the time lag becomes longer, with the largest drop from a 1-day to a 2-day lag. The correlation of the ozone and CO fields with 2–3 or more days apart

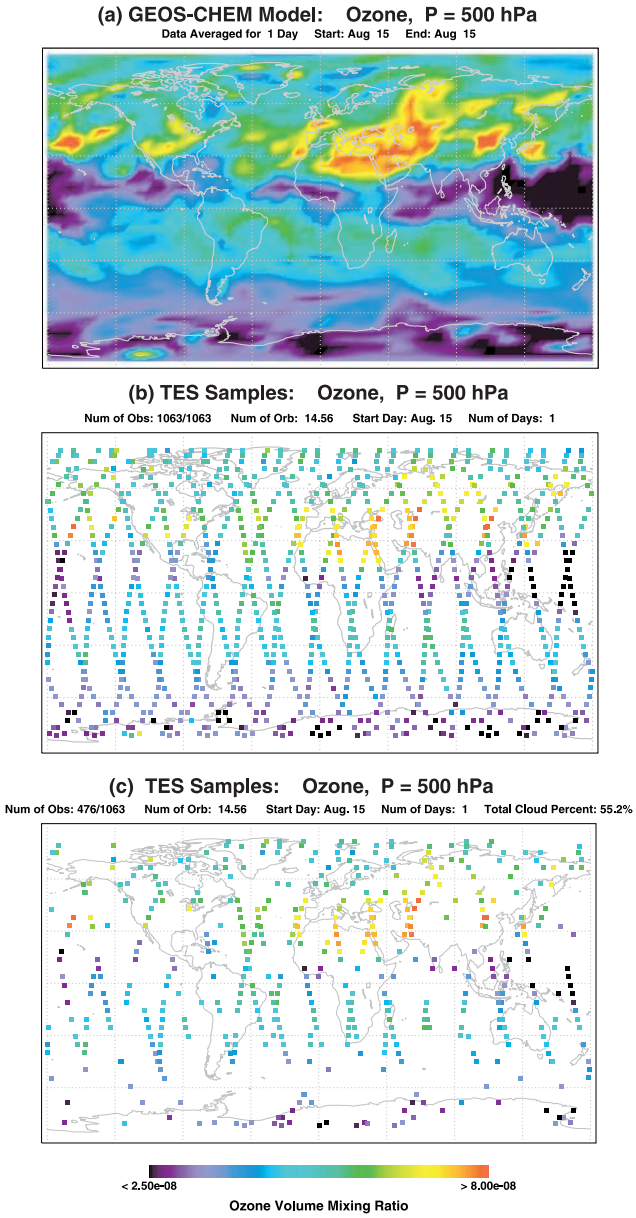

Figure 1. Global ozone volume mixing ratio field at 500 hPa for 15 August 1994 from the GEOS-CHEM model. (a) The daily average field. (b) The Tropospheric Emission Spectrometer (TES) nadir observation ground track obtained via temporal-spatial sampling through the model fields (total of 1063 observations). (c) The TES nadir observation ground track locations with those having clouds in the view removed (total of 476 observations). The actual nadir footprint is $\sim 5 \times 8$ km.

becomes small. This analysis suggests that with the limitation of the satellite orbit progression and the required 50% observation time for TES a sampling strategy of mapping the global ozone and CO fields every 2–3 days would be appropriate.

[9] The above global model field analysis suggests a 1-day-on followed by a 1-day-off pattern for TES global survey observations, producing ozone and CO daily global maps every other day. This global survey does not preclude targeted observations for specific regions on the off days to address special events or intense regional survey modes. The planned validation campaigns can also be accommodated in the off days. In the next three sections we follow three steps to simulate TES final products, the daily global species fields, and to compare them with the model true atmospheres.

3. Sampling the Troposphere Along the TES Orbit Track

[10] The EOS Aura polar orbit is Sun synchronous at 705 km with 98.2° inclination. Each TES observation sequence includes two nadir scans pointing at the same ground location and three trailing limb scans. For observations taken equatorward of 70° latitude the local solar times are within 3 hours after noontime for the ascending track and within 3 hours after midnight for the descending track. There are 73 observation sequences per orbit and ~14.5 orbits per day. The size of 1 pixel at nadir is ~5 km × 0.5 km, and the size of 16 stacked pixels at nadir is ~5 km × 8 km.

[11] The TES nadir footprints along the orbit track are used to sample the species profiles from the model fields. The model profiles adjacent to the footprints are linearly interpolated in time and bilinearly interpolated in space to obtain the sampling profile at a TES footprint. Figure 1b shows the TES nadir location for 1 day (14.56 orbit) colored by the sampled ozone volume mixing ratio at 500 hPa. This plot clearly illustrates the limitations of the spatial resolution of the TES observations. Small features in the species fields (less than ~15° longitude and ~5° latitude) are unlikely to be captured by TES observations. Careful examination of the animations of the model fields shows that small features tend to move fast. Considering that Figure 1b is not a snapshot of the field, the low temporal resolution of the observations also limits the ability of TES to capture the rapidly evolving small-scale features in a field.

[12] The presence of clouds in the TES field of view is an issue in profile retrieval. Although the TES science team has developed algorithms to retrieve profiles down to the cloud top in the nadir viewing case, the retrieval results will need careful validation when data become available. Partial cloud cover in 1 or all 16 pixels is especially hard to deal with. In this paper, we assume therefore that there is no retrieved profile at the TES footprint when a cloud is in the field of view as indicated by the GEOS total cloud fraction [*Takacs et al.*, 1994]. We treat the GEOS cloud fraction as a probability that the TES field of view in a given grid square samples a cloudy scene. As an example, Figure 2 shows the cloud probabilities above three specified levels for 15 August at 0000 UT. Removing all cloudy scenes (Figure 2c) filters out 55% of the observations for this day, which is a significant reduction. However, large-scale structures in ozone volume mixing ratios are still captured in the samples retained, as shown in Figure 1c.

4. Simulated Retrievals and Error Estimate on the Sampled Profiles

[13] The model fields, temporally and spatially sampled along the TES orbit track footprints, become the true

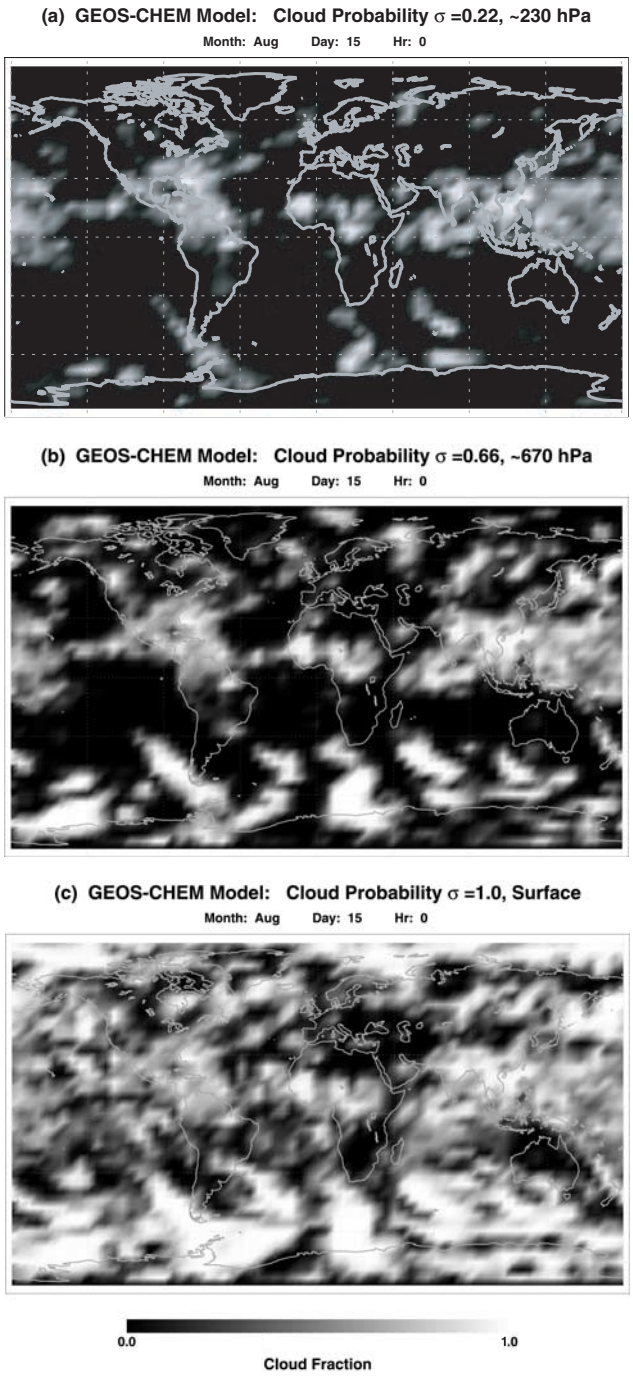

Figure 2. Global cloud fractions above a given level as diagnosed by the Global Earth Observing System (GEOS)-assimilated meteorological observations for 15 August 1994. (a) Above $\sigma = 0.22$, ~230 hPa. (b) Above $\sigma = 0.66$, ~670 hPa. (c) Above $\sigma = 1.0$, the surface of the earth.

profiles for evaluating TES retrieval products. For operational processing, atmospheric profiles will be retrieved from the spectral radiances according to the process described in the TES Algorithm Theoretical Basis Document (available at the EOS Aura project home page, http://aura.gsfc.nasa.gov/) using a nonlinear least squares process. Ideally, to simulate the observing system, we would calculate the spectra to be measured, including noise, and then carry out the operational retrieval. However, this would be expensive in processor time at the current stage of development of the operational retrieval. An alternative process is to simulate the combination of measurement and retrieval by means of a linear characterization. Although the retrieval process is nonlinear, this should give a qualitative evaluation of the effect of retrieval on global maps.

[14] *Rodgers* [1990] presents a suitable formalism for this purpose. The retrieved profile $\hat{x}$ is related to the true profile x to first order by a relation of the form

$$\hat{x} = Ax + (I - A)x_a + G\varepsilon, \tag{2}$$

where I is the unit matrix, G is the retrieval gain (contribution function), ε is the measurement noise, and A is the averaging kernel matrix. A describes the sensitivity of the retrieval to the true state. Equation (2) describes the retrieval as a linear combination of the true profile smoothed by the averaging kernel and the prior profile x_a weighted by $I - A$, together with the contribution from measurement error $G\varepsilon$. Systematic errors in the forward model can be included as a component of ε, but we have not done so in this study. The averaging kernel matrix is computed as $A = GK$. The Jacobian matrix K (the derivative of the model spectrum with respect to the species profile), the retrieval gain G, and the measurement noise covariance S_m are the key characteristics of TES observations that determine the vertical resolution and the error of the retrieved profiles. The retrieval gain G depends upon the covariance S_a of the prior state about its expected value x_a, according to *Rodgers* [1976].

$$G = (K^T S_m^{-1} K + S_a^{-1})^{-1} K^T S_m^{-1} \tag{3}$$

We have taken S_m to be diagonal.

[15] The advantage of the high throughput (adequate signal-to-noise ratio) of a Fourier transform spectrometer makes high spectral resolution measurement of a large spectral range possible, which is ideal for tropospheric/stratospheric species profile measurements. Detailed discussions of the TES radiative transfer forward model, nadir retrieval simulations, and error analyses are given by *Clough et al.* [1995] and *Bowman et al.* [2002]. Here the TES forward model is used to evaluate the Jacobian matrix K at x_a using spectral regions centered near 9.6 μm for ozone and 4.7 μm for CO. The use of a priori covariance S_a or other implicit constraints for retrieval are necessary to obtain physically meaningful results for the ill-posed profile retrieval problem.

[16] For our simulations the appropriate sources of x_a and S_a are the annual statistics of the three-dimensional model results. We chose not to include seasonal information in the prior state as this may be misleading, e.g., with regard to the timing of biomass burning events. Gross latitudinal variation was included, however. We chose four latitude bands for which to calculate the annual mean state x_a and the covariance S_a about it, namely, 90°S–20°S, 45°S–10°N, 10°S–45°N, and 20°N–90°N. These were used as a priori for profile retrievals for 90°S–30°S, 30°S–0°, 0°–30°N, and 30°N–90°N, respectively. The four tropospheric profiles are extended smoothly to the upper stratosphere using latitudinal dependent ozone profiles from the Air Force

Geophysics Laboratory reference atmospheric model profiles [*Anderson et al.*, 1986].

[17] Figures 3a and 3b show the annual averages of the ozone profiles from the GEOS-CHEM model for the four latitude bands and an example of a covariance matrix. Retrieval in terms of the logarithm of the mixing ratio q is currently under consideration for the TES retrieval algorithm, so in this study the state vector elements x_a are taken to be $\ln(q)$. The element jk of the covariance matrix S_a is the covariance of the logarithm of the mixing ratios at level j with that at level k, and it is

$$S_{jk} = (n-1)^{-1} \sum_{i=1}^{n} (x_{ij} - x_{aj})(x_{ik} - x_{ak}). \quad (4)$$

The summation is over all model profiles within the latitude band, and n is the total number of data points. It might be expected that, as the model has 14 levels and the retrieval is at 21 levels, the prior covariance would be of rank 14, and therefore singular. However, since the model uses sigma levels, which vary in pressure from one profile to another and in $\ln(q)$ is performed on $\ln(p)$ before the data is used, this is not the case. However, variability at scales smaller than the model resolution cannot be well captured by this S_a. In the stratosphere, S_a is assumed to be diagonal with constant values at the tropopause.

[18] The prior information for the four latitude bands is used to calculate the parameters of the simulated retrieval, (2) and (3). The measurement error is an important factor in demonstrating the capability of the TES measurements. We have used the current best estimate for a single-pixel measurement, namely 2.24×10^{-4} W m^{-2} sr^{-1} cm^{-1} for all the simulations. If measurements from up to 16 pixels are averaged for nadir retrievals, the random measurement error will be reduced by a factor of 4. The Jacobian matrices K are calculated for the four latitude bands using the appropriate x_a.

[19] Figure 3c illustrates an example of the averaging kernel matrix, $A = KG$, used for retrieval simulations in (2). The rows of A matrix are plotted against pressure for every other retrieval pressure levels between 1000 and 100 hPa. Each averaging kernel profile is used to vertically smooth the true profile for a given retrieval level as indicated in (2).

[20] The total retrieval error covariance is estimated according to *Rodgers* [1976].

$$\hat{S} = (K^T S_m^{-1} K + S_a^{-1})^{-1} \quad (5)$$

This error includes the contribution from measurement noise together with the smoothing error corresponding to the variability of the profile that can be represented in the model data but cannot be determined from the observations. Other sources of errors are not considered here. The effect of temperature profile error on the ozone retrieval is discussed by *Clough et al.* [1995].

[21] The fast retrieval (2) is applied to all of the sampled profiles at TES footprints that are cloud free. A total of over 170,000 "retrievals" per species per year were performed in this way to become our simulated level 2 products. To validate the process we also carried out "real" simulated retrievals using the TES prototype retrieval code for a small sample of profiles. The majority of the results agree very

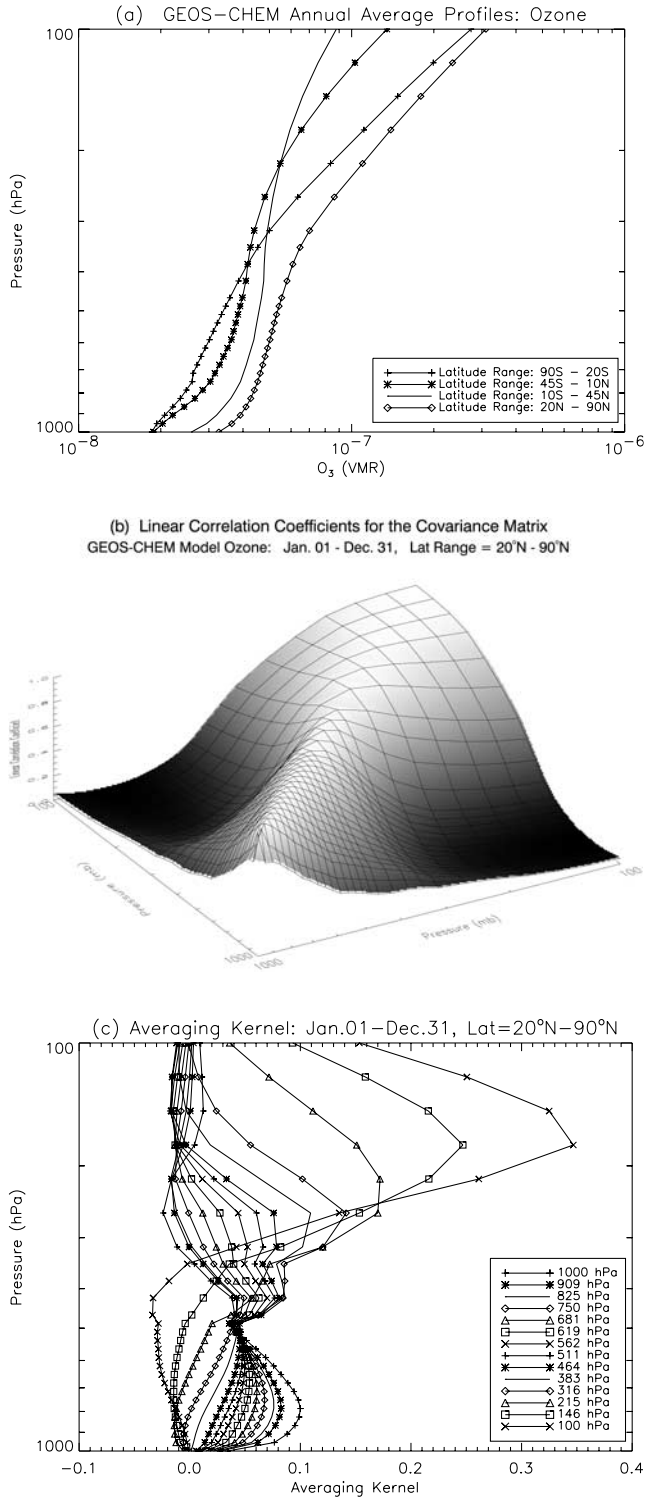

Figure 3. A priori information obtained from the GEOS-CHEM yearlong model data for ozone. (a) Annual average profiles for the four latitude bands (used as a priori states x_a for the simulated retrievals). (b) Linear correlation coefficients for the covariance matrix obtained from the vertical ozone profiles in the latitude band 20°N–90°N (S_a). (c) Averaging kernels (rows of the A matrix) for the ozone retrieval at 20°N–90°N. This plot only shows alternate rows of the averaging kernel matrix, while the retrievals are performed at all levels (total of 21 levels).

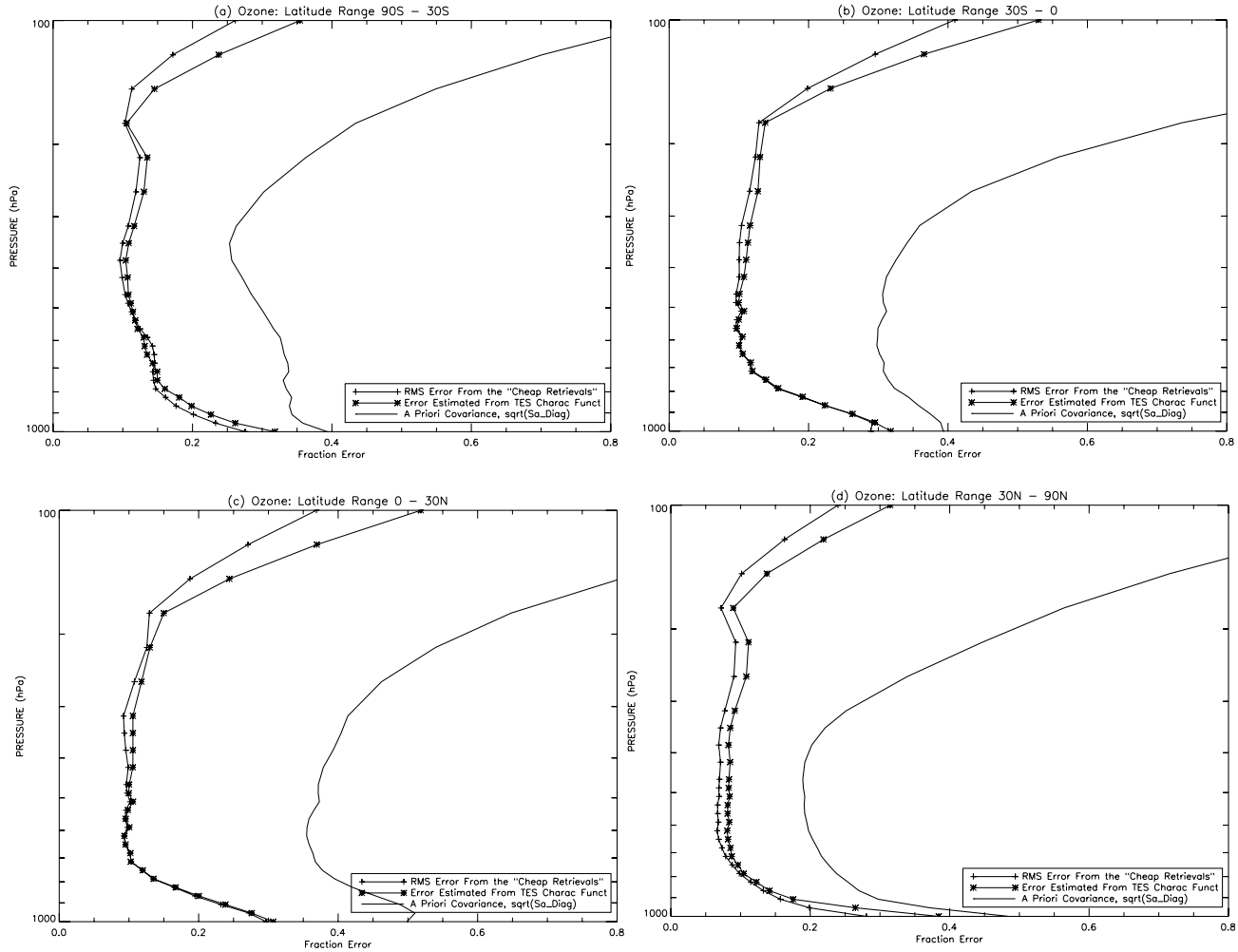

Figure 4. Fractional errors for ozone retrieval in the four latitude bands, (a) 90°S–30°S, (b) 30°S–0°S, (c) 0°N–30°N, and (d) 30°N–90°N. There are three profiles in each panel: the RMS of the retrieval errors obtained from the departures of the retrieved profiles from the "true" profiles, the square root of the diagonals of the estimated retrieval error covariance matrix $\hat{S}$, and the square root of the diagonals of the a priori covariance matrix S_a.

well with the simulations. More profile retrieval simulations for the TES instrument are given by *Clough et al.* [1995] and *Bowman et al.* [2002].

[22] Figures 4a–4d demonstrate the comparison between the retrieval error and the a priori variance for the four latitude bands. The retrieval errors are calculated in two ways, (5) and the RMS of the departures of the retrieved profiles $\hat{x}$ from their true profiles x. The RMS is calculated using over 170,000 retrievals. As expected, the agreement between the RMS error and the estimated S is excellent. In general, the retrieval error for annual averaged ozone in a wide latitude band is 8–15% from ~800 to 200 hPa, with higher values near the surface and the tropopause. Using 16 pixel-averaged measurements, this retrieval error can be reduced to 5–10% in most parts of the troposphere. *Clough et al.* [1995] estimated 5% retrieval error in the middle-upper troposphere for a 32 pixel-averaged measurement and a slightly different S_m. This value is in good agreement with this study.

[23] Knowledge of the vertical resolution or the number of vertically independent pieces of information in the retrieved species profile is important to understand the TES products and the estimated errors. This vertical resolution can be described as the width of the row of the averaging kernel matrix A. Equation (2) indicates that the retrieved profile is the sum of the smoothed true profile via the rows of A and other two terms. As illustrated in Figure 3c, the width of the averaging kernel for the simulated ozone retrieval here is ~5–8 km in the troposphere. We therefore estimate that among the 21 levels used to represent the ozone profile in the troposphere, there are only 2–3 pieces of independent information.

[24] The above-described retrieval simulation was also performed for carbon monoxide for the Southern and Northern Hemispheres. With similar retrieval errors (~10% in the lower-middle troposphere for a single pixel), ~2 pieces of vertically independent information can be obtained for CO.

5. Level 3 Mapping and Comparison to the Model Fields

[25] Global image maps of the species field at a constant pressure level (or constant potential temperature level) will

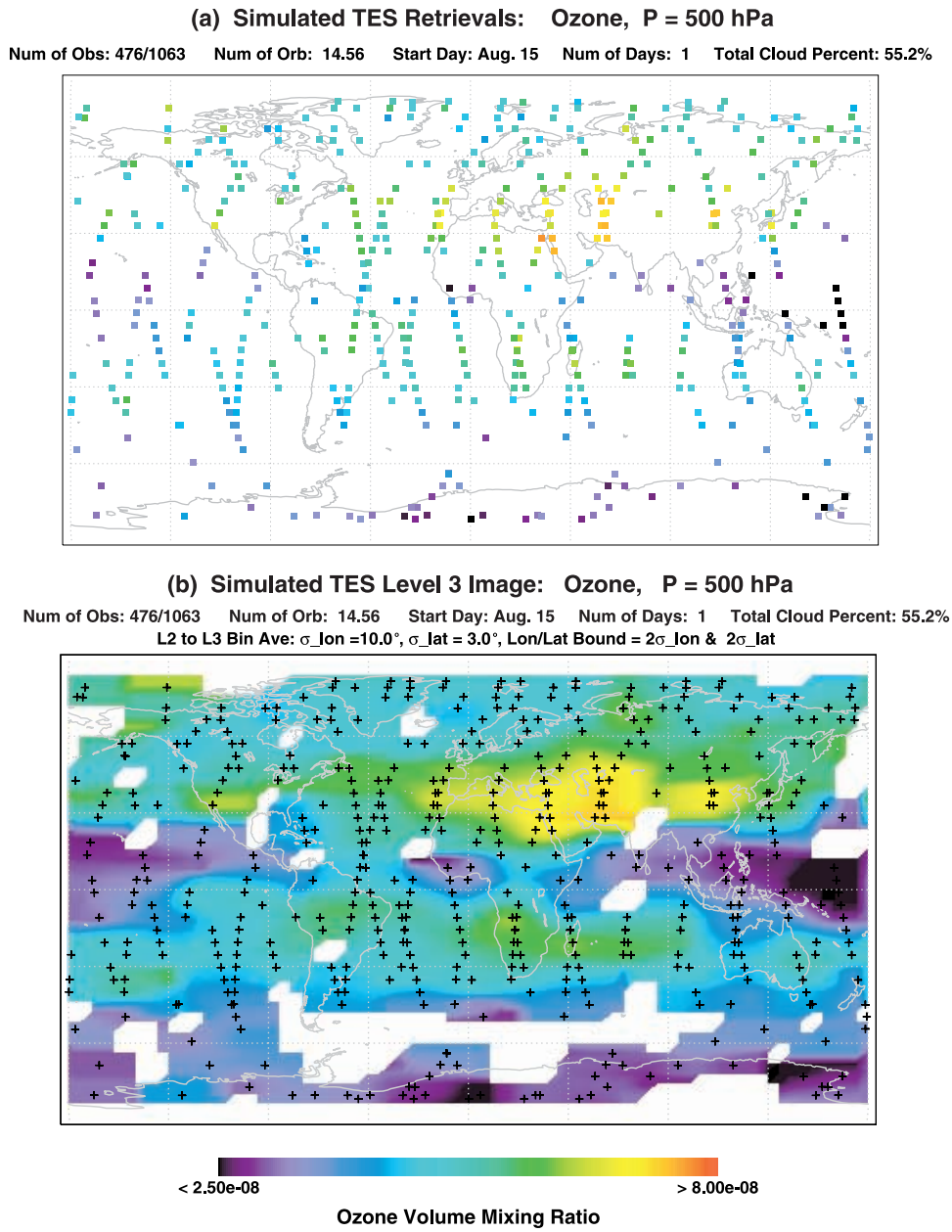

Figure 5. The global ozone volume mixing ratio fields at 500 hPa for 15 August 1994. (a) Retrieved ozone volume mixing ratio at TES nadir footprints using a fast retrieval algorithm described in section 3. (b) Global level 3 map obtained using a simple Gaussian weight-binning method. This figure is the continuation of Figure 1. Some statistics comparing the level 3 image (Figure 5b) and the original model image (Figure 1a) are given in Table 1.

be the core products from TES level 3 processing. These level 3 maps are mainly for data browsing. Similar to all the remote-sensing observations from a polar-orbit satellite, TES footprints cover most latitudes in ~1 day. Studies in section 3 show that the TES nadir coverage in the lower troposphere is complicated by ~50–60% of data being lost due to clouds in the view. As an example, Figure 5a shows the TES nadir footprints for the 15 August model fields, with colors representing the retrieved ozone mixing as described in section 4. An important consideration in producing a global image from the data in Figure 5a is that there is an offset of up to 1 day between the different data points. Several techniques exist to generate quasisynoptic maps from the above-described asynoptic observations [*Salby*, 1982]. They can be generalized as time/space interpolations. This step of processing imposes smoothing to the time/space evolutions of the fields and has difficulty in dealing with data gaps. Data assimilation with a global 3-D tropospheric chemistry model such as GEOS-CHEM would provide a solution, but it is a complex undertaking and is inappropriate for a browse product. In this study we use a simple mapping algorithm described below to generate daily gridded level 3 data, ignoring timing offsets. The level 3 grid is defined to sample the field structures

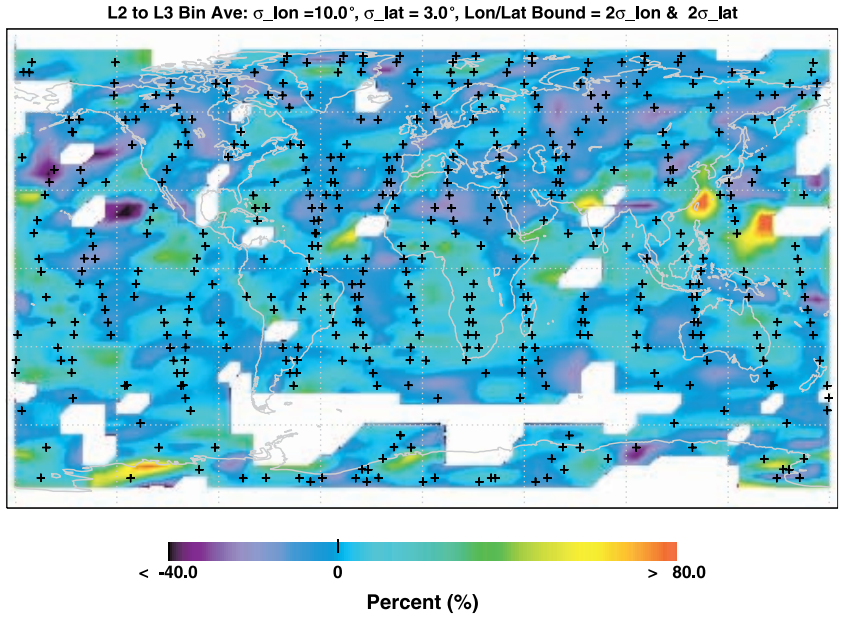

Figure 6. Percent difference of level 3 data from the model daily average data for the ozone field at 500 hPa on 15 August 1994. The level 3 data is displayed in Figure 5b, and the model data is displayed in Figure 1a.

captured by the orbit footprints, for example, a 5° longitude × 2° latitude grid is a reasonable selection for a daily map considering the TES sampling spatial resolution. First, level 2 data are accumulated for a period of time, e.g., 1-day observations shown in Figure 5a. Then a bin box centered at the specified level 3 grid is defined. The size of the bin box is determined by the spatial distribution of the data, and it represents the area of influence of a given data point. The level 2 data within the range of the bin are used for averaging, and each data point is weighted by a 2-D Gaussian function centered at the level 3 grid point. In the case of no data for level 2 in the bin box, there will be no level 3 data at that grid point. As an example, Figure 5b shows the level 3 map for ozone mixing ratio at 500 hPa using the 1-day level 2 data shown in Figure 5a.

[26] The difference between the binned data and the model fields should give us a semiquantitative idea of the magnitude of the errors due to three major sources: the TES orbit sampling, the level 2 retrieval, and the level 3 mapping. As an example, the percent differences of the level 3 global map (Figure 5b) from the model daily average field (Figure 1a) for the ozone field at 500 hPa on 15 August is shown in Figure 6. It is important to point out that the error field seems to be random; it shows no significant patterns, such as the orbit track, nor does it correlate with the original field. Table 1 presents more quantitative analyses of the three error sources in this field. To account for the model field variability in its daily map, we have calculated the percent RMS of the departure of the 6 daily 4-hour fields from the daily average field (Table 1). For ~90% of the global area this RMS difference is <10%, while for ~8% of the global area it is 10–20%. These values perhaps represent the maximum error due to the TES orbit sampling of the ozone field and the assumption of a constant field. Table 1 examines the error in level 3 mapping when the simple mapping method described above is applied to the orbit sampled true atmosphere profiles. This error is <10% for 78% of the domains. This drop in area represents the error due to the level 3 interpolation. The effects of the retrieval with approximate 10% error at 500 hPa (Figure 4) are included in Table 1. The simulated retrieval profiles are used to generate level 3 maps. With all three error sources included, Table 1 shows that for 75% of the global area the percent difference between level 3 and the model is <10%, and for another 15% of the global area the percent difference is 10–20%.

[27] Two more examples of the comparisons of the level 3 maps and the true model fields are shown in Figure 7, and the statistical errors are included in Table 1. Figures 7a and 7b and Table 1 show the simulation for the ozone field at 800 hPa on 15 August. Although the macrostructures of the field are captured by the global level 3 map, the strength of the ozone sources due to biomass burning in the two southern continents are underestimated by the simulated TES data. The high retrieval error near the surface (Figure 4) is the major reason. With only two to three pieces of

Table 1. Error Estimates for Three Sample Fields[a]

	O_3 for 15 August 1994		CO for 20 February 1994,
	500 hPa, %	800 hPa, %	700 hPa, %
Area, %			
$\Sigma_0 < 10$	90	85	93
$10 < \Sigma_0 < 20$	8	12	6.5
$\Sigma_1 < 10$	78	72	81
$10 < \Sigma_1 < 20$	14	14	11
$\Sigma_2 < 10$	75	67	75
$10 < \Sigma_2 < 20$	15	12	14
Retrieval error	10	15	10

[a] Σ_0, RMS of departures of model species volume mixing ratio (VMR) from the daily mean. Σ_1, departure of level 3 map generated from orbit sampled "true atmosphere" and the model daily mean VMR. Σ_2, departure of level 3 map generated from retrieved level 2 daily data and the model daily mean VMR.

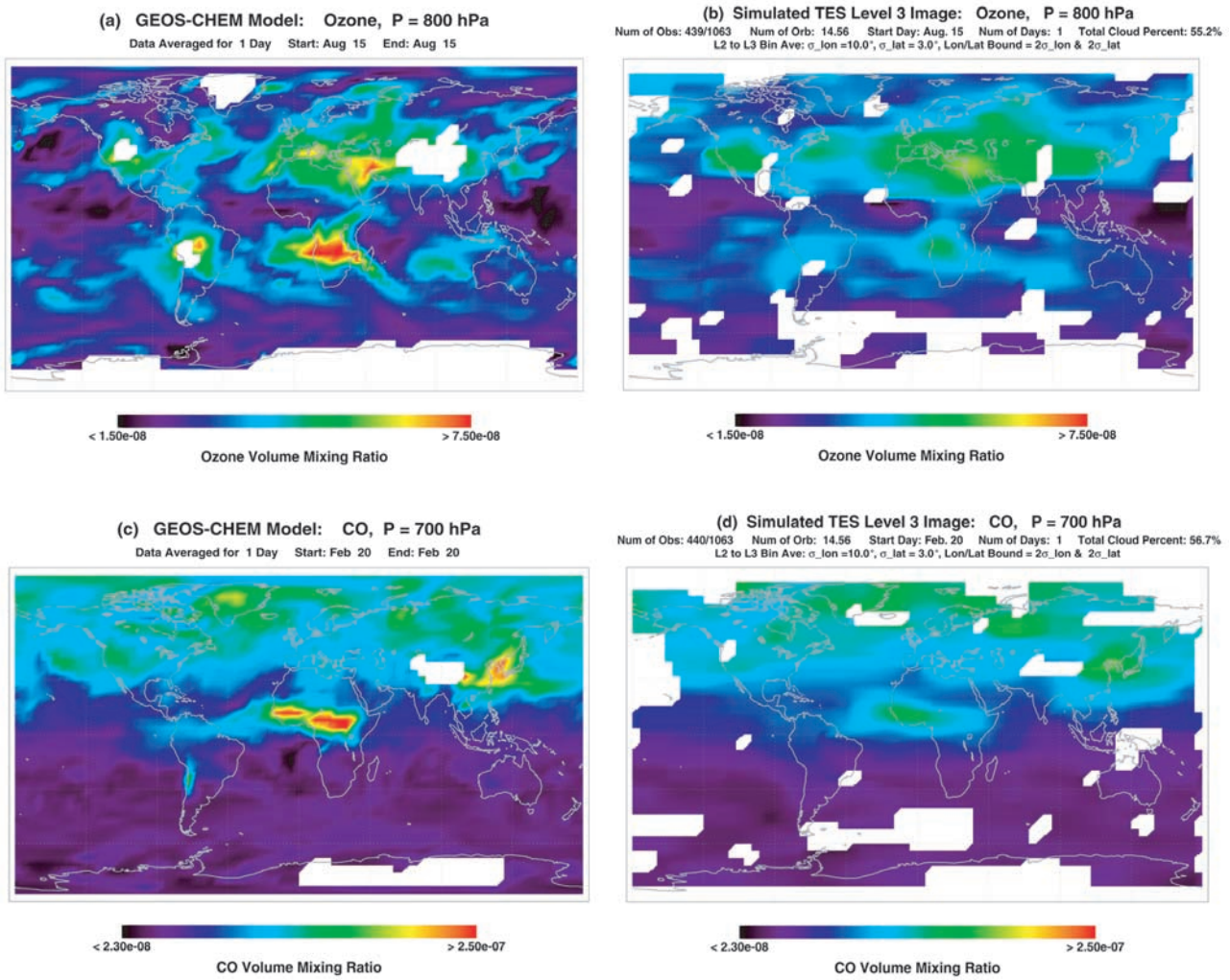

Figure 7. Comparisons of the GEOS-CHEM fields and the simulated TES level 3 maps. (a and b) Ozone volume mixing ratio at 800 hPa for 15 August. (c and d) CO volume mixing ratio field at 700 hPa for 20 February 1994.

information vertically in the tropospheric retrieved profiles the variability represented in the model profiles is vertically smoothed in the retrieval process of the observations. Such ozone profiles departing from the regional climatology impose challenges to TES retrieval algorithms, including the proper ways of using a priori profiles and the smoothness constraints to the profiles. Another example shown in Figures 7c and 7d and Table 1 is the level 3 map versus model field for CO at 700 hPa on 20 February 1994. Again, the large global features are captured well by the level 3 map, while the magnitudes of the high-CO regions due to pollution sources are not reproduced well. Note that in this case the evolution of the CO fields in East Asia and North Africa is rapid, and the percent RMS of the departure of the model 4-hour fields (not shown here) from the daily mean in these regions is as high as 35%. This sampling error has major contributions to the departure of the level 3 field from the model daily field.

[28] The error due to the level 3 mapping described here seems to be significant, but it can be reduced using smaller bin size while sacrificing the visual appearance. Other local interpolation algorithms are under consideration for producing level 3 browse products. However, with such sparse observations globally and a similar influence area for a given data point the mapping error is predictable. TES data assimilation with a global dynamic chemistry model should provide the most probable global time-varying state for ozone, CO, and other tropospheric species. Such data assimilation using models has been reported for other satellite observations, e.g., the MAPS and MOPITT CO observations [*Lamarque et al.*, 1999] and the global total ozone column from GOME (available at http://auc.dfd.dlr.de/GOME/products/). We propose to produce assimilated data as TES future higher-level products.

[29] The tools and analyses described in this paper allow the TES science team to make decisions on the sampling strategies for the global survey observations. A 1-day global map seems to capture adequately the macrofeatures in the ozone and other slowly varying fields such as CO, H_2O, and temperature, even with ~55% data missing due to clouds. Although the measurement accumulated for a longer period (e.g., 2 days or more) should fill some of the empty areas, it will increase the error in these level 3 maps due to the temporal variation of the true field.

6. Summary and Conclusions

[30] This paper uses results from the GEOS-CHEM global 3-D model of tropospheric chemistry as a synthetic atmosphere to define the TES global observational strategy and to investigate the ability of TES observations to capture the tropospheric structure of ozone and CO. A significant autocorrelation at 1 day is identified from the model fields in the troposphere (coefficient = 0.5–0.6). This coefficient is a factor of 2 smaller for 2-day or longer time lags. Considering the limitation of a 50% duty cycle, this study suggests a sampling strategy of 1-day-on followed by 1-day-off for TES global survey observations.

[31] The GEOS-CHEM model fields along with the corresponding cloud information were used as a synthetic ''true'' atmosphere to generate simulated TES products and to evaluate the TES observation capability. First, the model fields were sampled along the TES orbit track. Then the model cloud fields are used to screen and reject cloudy footprints in the field of view of the instrument. Although the cloud top levels for those footprints are also known, in the examples shown in this paper we simply remove all cloudy profiles. This conservative approach is based on the expectation that retrieval in cloudy atmosphere will need extensive validation after launch. The next step is to perform a retrieval of the clear-sky GEOS-CHEM model profiles to generate global level 2 products. An approximate retrieval based on those true profiles and the TES characteristic functions is performed for a whole year's data. This procedure is basically to smooth the true profile vertically by the averaging kernels and to add the effect of the instrument noise. The application of necessary smoothing results in two to three pieces of independent information for a retrieved ozone profile in the troposphere. An error analysis is also provided, and for most of the troposphere this error is ~10–15% using the single pixel noise. The last step is to produce level 3 species maps and to compare with the true time-varying model field. A simple Gaussian function weighted-binning method is used to generate level 3 data. The daily global level 3 maps for the ozone and CO fields are compared to the model fields. The comparisons show that the error is <10% in ~70% global area and <20% in 80–90% area.

[32] The prelaunch quantitative assessments of simulated TES final products compared to global atmospheric chemistry model fields used as true atmosphere are useful in planning the observation strategy. This study also offers an example for future TES data users to better understand the limitations and the error sources of the data and the global maps. On the basis of this study and other sources of inputs, an alternating 1-day-on and 1-day-off mode has been identified as the TES primary sampling strategy for global surveys. Global daily maps for tropospheric species such as ozone, CO, and H_2O will be generated every other day.

[33] **Acknowledgments.** We thank all members of the TES science and software engineering team for their support on this study. We also thank M. Schoeberl for initiating this study. We specially thank B. Field for providing the GEOS-CHEM model data and S. A. Clough, D. Rider, H. Worden, A. Eldering, D. Tremblay, and J. Wright for many helpful discussions. The research described in this paper was carried out at the Jet Propulsion Laboratory, California Institute of Technology, under a contract with the National Aeronautics and Space Administration.

References

Anderson, G. P., S. A. Clough, F. X Kneizys, J. H. Chetwynd, and E. P. Shettle, AFGL atmospheric constituent profiles (0–120 km), *Tech. Rep. AFGL-TR-86-0110*, Phillips Lab., Hanscom Air Force Base, Mass., 1986.

Beer, R., T. A. Glavich, and D. M. Rider, Tropospheric Emission Spectrometer for the Earth Observing System's AURA satellite, *Appl. Opt.*, *40*, 2356–2367, 2001.

Bey, I., D. J. Jacob, R. M. Yantosca, J. A. Logan, B. Field, A. M. Fiore, Q. Li, H. Liu, L. J. Mickley, and M. Schultz, Global modeling of tropospheric chemistry with assimilated meteorology: Model description and evaluation, *J. Geophys. Res.*, *106*, 23,073–23,095, 2001.

Bowman, K. W., T. Steck, H. M. Worden, J. Worden, S. Clough, and C. D. Rodgers, Capturing time and vertical variability of tropospheric ozone: A study using Tropospheric Emission Spectrometer nadir retrieval, *J. Geophys. Res.*, *107*, 10.1029/2002JD002150, in press, 2002.

Clough, S. A., C. P. Rinsland, and P. D. Brown, Retrieval of tropospheric ozone from simulations of nadir spectral radiances as observed from space, *J. Geophys. Res.*, *100*, 16,579–16,593, 1995.

Drummond, J. R., and G. S. Mand, The measurements of pollution in the troposphere (MOPITT) instrument: Overall performance and calibration requirements, *J. Atmos. Oceanic Technol.*, *13*, 314–320, 1996.

Fishman, J., C. E. Watson, J. C. Larson, and J. A. Logan, Distribution of tropospheric ozone determined from satellite data, *J. Geophys. Res.*, *95*, 3599–3617, 1990.

Fowler, L. D., B. A. Wielicki, D. A. Randall, M. D. Branson, G. G. Gibson, and F. M. Denn, Use of a GCM to explore sampling issues in connection with satellite remote sensing of the Earth radiation budget, *J. Geophys. Res.*, *105*, 20,757–20,772, 2000.

Hadji-Lazaro, J., C. Clerbaux, and S. Thiria, An inversion algorithm using neural network to retrieve atmospheric CO concentrations form high-resolution nadir radiances, *J. Geophys. Res.*, *104*, 23,841–23,854, 1999.

Horowitz, L. W., and D. J. Jacob, Global impact of fossil fuel combustion on atmospheric NO_x, *J. Geophys. Res.*, *104*, 23,823–23,840, 1999.

Lamarque, J. F., B. V. Khattatov, J. C. Gille, and G. P. Brasseur, Assimilation of Measurement of Air Pollution from Space (MAPS) CO in a global three-dimensional model, *J. Geophys. Res.*, *104*, 26,209–26,218, 1999.

Li, Q., D. J. Jacob, J. A. Logan, I. Bey, R. M. Yantosca, H. Liu, R. V. Martin, A. M. Fiore, and V. Thouret, A tropospheric ozone maximum over the Middle East, *Geophys. Res. Lett.*, *28*, 3235–3238, 2001.

Logan, J. A., Ozone in rural areas of the United States, *J. Geophys. Res.*, *94*, 8511–8532, 1989.

Mickley, L. J., P. P. Murti, D. J. Jacob, J.A. Logan, D. Rind, and D. Koch, Radiative forcing from tropospheric ozone calculated with a unified chemistry-climate model, *J. Geophys. Res.*, *104*, 30,153–30,172, 1999.

Munro, R., R. Siddans, W. J. Reburn, and B. J. Kerridge, Direct measurement of tropospheric ozone distributions from space, *Nature*, *392*, 168–171, 1998.

Reichle, H. G., Jr., et al., Space shuttle based global CO measurements during April and October 1994, MAPS instrument, data reduction, and data validation, *J. Geophys. Res.*, *104*, 21,443–21,454, 1999.

Rodgers, C. D., Retrieval of atmospheric temperature and composition from remote measurements of thermal radiation, *Rev. Geophys.*, *14*, 609–624, 1976.

Rodgers, C. D., Characterization and error analysis of profiles retrieved from remote sounding measurements, *J. Geophys. Res.*, *95*, 5587–5595, 1990.

Salby, M. L., Sampling theory for asynoptic satellite observations, I, Space-time spectra, resolution, and aliasing, *J. Atmos., Sci.*, *39*, 2577–2600, 1982.

Takacs, L. L., A. Molod, and T. Wang, Documentation of the Goddard Earth Observing System (GEOS) general circulation model—Version 1, *Tech. Memo. 104606*, Natl. Aeronaut. and Space Admin., Washington, D.C, 1994.

Wang, Y., D. J. Jacob, and J. A. Logan, Global simulation of tropospheric O_3-NO_x-hydrocarbon chemistry, 1 Model formulation, *J. Geophys. Res.*, *103*, 10,713–10,726, 1998a.

Wang, Y., J. A. Logan, and D. J. Jacob, Global simulation of tropospheric O_3-NO_x-hydrocarbon chemistry, 2, Model evaluation and global ozone budget, *J. Geophys. Res.*, *103*, 10,727–10,756, 1998b.

R. Beer and M. Luo, Jet Propulsion Laboratory, California Institute of Technology, MS 183-301, 4800 Oak Grove Dr., Pasadena, CA 91109, USA. (beer@tes-mail.jpl.nasa.gov; Ming.Luo@jpl.nasa.gov)

D. J. Jacob and J. A. Logan, Department of Earth and Planetary Sciences, Harvard University, Pierce Hall, 29 Oxford Street, Cambridge, MA 02138, USA. (djj@io.harvard.edu; jal@io.harvard.edu)

C. D. Rodgers, Atmospheric, Oceanic and Planetary Physics, University of Oxford, Oxford, OX1 2JD, UK. (c.redgers@physics.ox.ac.uk)